ARMY RESEARCH LABORATORY

Modeling Microfabricated Multipoint Fuze Initiators Part 1: Pre-Melting Behavior

by Christopher J. Morris, Eugene Zakar, Brian Mary, Edward Shaffer, Paul Amirtharaj, and Madan Dubey

ARL-TR-4371 **January 2008**

NOTICES

Disclaimers

The findings in this report are not to be construed as an official Department of the Army position unless so designated by other authorized documents.

Citation of manufacturer's or trade names does not constitute an official endorsement or approval of the use thereof.

Destroy this report when it is no longer needed. Do not return it to the originator.

Army Research Laboratory
Adelphi, MD 20783-1197

ARL-TR-4371 **January 2008**

Modeling Microfabricated Multipoint Fuze Initiators Part 1: Pre-Melting Behavior

Christopher J. Morris, Eugene Zakar, Brian Mary
Edward Shaffer, Paul Amirtharaj, and Madan Dubey
Sensors and Electron Devices Directorate, ARL

REPORT DOCUMENTATION PAGE

Form Approved
OMB No. 0704-0188

1. REPORT DATE *(DD-MM-YYYY)*	2. REPORT TYPE	3. DATES COVERED (From - To)
January 2008	Final	

4. TITLE AND SUBTITLE
Modeling Microfabricated Multipoint Fuze Initiators Part 1: Pre-Melting Behavior

5a. CONTRACT NUMBER

5b. GRANT NUMBER

5c. PROGRAM ELEMENT NUMBER

6. AUTHOR(S)
Christopher J. Morris, Eugene Zakar, Brian Mary, Edward Shaffer, Paul Amirtharaj, and Madan Dubey

5d. PROJECT NUMBER

5e. TASK NUMBER

5f. WORK UNIT NUMBER

7. PERFORMING ORGANIZATION NAME(S) AND ADDRESS(ES)
U.S. Army Research Laboratory
ATTN: AMSRD-ARL-SE-RL
2800 Powder Mill Road
Adelphi, MD 20783-1128

8. PERFORMING ORGANIZATION REPORT NUMBER
ARL-TR-4371

9. SPONSORING/MONITORING AGENCY NAME(S) AND ADDRESS(ES)
U.S. Army Research Laboratory
2800 Powder Mill Road
Adelphi, MD 20783-1128

10. SPONSOR/MONITOR'S ACRONYM(S)

11. SPONSOR/MONITOR'S REPORT NUMBER(S)

12. DISTRIBUTION/AVAILABILITY STATEMENT
Approved for public release; distribution unlimited.

13. SUPPLEMENTARY NOTES

14. ABSTRACT
Future combat systems require warheads with multi-point initiators to produce precise simultaneous detonations. Semiconductor fabrication methods, combined with MEMS-enabling process technologies at ARL, enable geometrically accurate conductors—bridge wire for such multi-point initiators. To understand how our device design, material deposition, and post processing influence bridge wire performance and ultimately simultaneity, we have simulated the behavior of an exploding metal bridge. In this report we present results focusing on the thermal-electric problem of heating up to the bridge wire melting point. The results in terms of time for the center of the exploding foil to reach the material melting temperature was within 2% of a similar, published modeling study, and approximately within 20% of the experimentally-observed time-to-burst for specific geometries fabricated at ARL. We also performed a sensitivity study and found the melting time to be most sensitive to bridge wire thickness, and all material properties except thermal conductivity. Simple, analytical arguments explain these results. Finally, we detail a path forward to eventually result in a predictive model allowing direct comparison between model outputs and experimental data. Such a model will greatly enhance our ability to design better bridge wire devices.

15. SUBJECT TERMS
Fuze initiator, finite element model

16. Security Classification of:			17. LIMITATION OF ABSTRACT	18. NUMBER OF PAGES	19a. NAME OF RESPONSIBLE PERSON
a. REPORT	b. ABSTRACT	c. THIS PAGE			Christopher J. Morris
U	U	U	U	34	19b. TELEPHONE NUMBER (*Include area code*) (301) 394-0950

Standard Form 298 (Rev. 8/98)
Prescribed by ANSI Std. Z39.18

Contents

List of Figures

List of Tables

1. Introduction

The behavior of an exploding metal initiator (a.k.a. exploding foil initiator, or slapper) has been studied extensively for single fuze detonator applications, but future combat systems (FCS) will require warheads with multi-point initiators that can produce simultaneous detonations. One can imagine the assembly of several resistor/conductor bridges of identical dimensions in an attempt to achieve the desired goal of simultaneous initiations, thus creating a maximum possible explosive force. However, variations of 1% in the resistivity, thickness uniformity, dimensions/volume, surface roughness and grain structures in the bridges can cause more than 50% variation in the initiator functionality, resulting in a very weak explosive force. The researchers at ARL have discovered a unique MEMS technology to prototype multiple Cu bridges (*1*, *2*) with less than 0.1% variation in the above mentioned parameters, thus creating the first multipoint fuzes that initiated with a high degree of simultaneity. The cost of these fuzes, when produced in quantity, is approximately one hundred times less than that of conventional fuzes.

This technology has several distinct advantages over conventional discrete technology. Typical discrete processes use thick-film screening printing, which limits bridge dimension accuracy to 100 μm and alignment resolution to 25 μm, and in turn reduces the desired explosive force. The use of semiconductor fabrication methods and MEMS-enabling process technologies yields an approximately 1000 times improvement in bridge dimension accuracy (0.1 μm tolerance) and repeatability of those dimensions across any number of points. This precision helps insure a high current-density flow path across a geometrically accurate conductor that will be shared equally amongst the points, contributing to a very high degree of simultaneity across an array.

The fuze community benefits from many years of experience modeling exploding foil initiators in terms of lumped parameter circuits, with parameters based primarily on empirical data fits. Several researchers have also employed finite element methods to predict the spatial temperature distribution in a metal bridge wire resulting from Joule heating, with model results generally valid up to the metal melting point (*4* through *7*). Pre-melt studies are important because simulations predict the metal to be in its solid phase for 90% of the time before reaching the experimentally-observed burst and departure of a flyer or slapper (*5*, *6*). Thus, it seems that the pre-melt temperature profile largely determines the post-melt and burst behavior, and the experimentally measured kinetic action of the flyer material.

To understand how our design or fabrication processes changes affect bridge wire performance and ultimately simultaneity, we have simulated the behavior of an exploding metal bridge. In

this report we present results following the methodology of others by focusing on the thermal-electric problem of the pre-melt phase. We have modeled the problem using material properties from two metals, Cu and Au. In future reports we plan to address post-melting phenomena as discussed in section 4.

2. Methods

2.1 Theory

The thermal-electric coupled problem is given by the equation from transient heat conduction,

$$c_v \rho_m \frac{\partial T}{\partial t} = \sigma_e \left|E\right|^2 + \nabla \bullet (k \nabla T) \tag{1}$$

and the equation for the electric field E,

$$\frac{\partial \rho_e}{\partial t} = E \bullet \nabla \sigma_e + \sigma_e \nabla E = 0, \tag{2}$$

where the electrical conductivity σ_e, thermal conductivity k, and specific heat c_v are all functions of temperature. The quantity $\partial \rho_e / \partial t$ relates to the diffusion of electrons in the metal, which is very short (*5*) and can be set to zero in equation 2.

It is often advantageous to non-dimensionalize equations prior to applying finite difference methods, in order to 1) avoid rounding errors in taking finite differences of very small numbers, and 2) to aid in presenting results and applying them to a more general set of experimental conditions. Non-dimensionalization involves choosing quantities for the fundamental units in the governing equations, which in equations 1 and 2 are time t, length L, mass m, temperature T, and charge C. Other quantities such as current I, thermal conductivity k, electrical conductivity σ_e, specific heat c_v (at constant volume), electric field E, or voltage V are related through these units as follows:

$$I = C / t \tag{3}$$

$$k = mL / t^3 T \tag{4}$$

$$\sigma_e = C^2 t / mL^3 \tag{5}$$

$$c_v = L^2 / t^2 T \tag{6}$$

$$E = mL / t^2 C \tag{7}$$

$$V = mL^2 / t^2 C \tag{8}$$

In order to generate non-dimensional variables for equations 1and 2 with values on the order of unity, we define:

$$t^* = t / t_I \tag{9}$$

$$L^* = L / a \tag{10}$$

$$T^* = \left[T - T_\infty\right] / \left[T_{\text{melt}} - T_\infty\right] \tag{11}$$

$$C^* = C / I_0 t_I \tag{12}$$

$$m^* = m / \left\{ \frac{I_0^2 t_I^3}{\left[\sigma_e\left(T_\infty\right)\right] a^3} \right\} \tag{13}$$

where t_I is the period of a sine wave for which the first half cycle represents the electrical input current pulse of amplitude I_0, a is the bridge wire width, $\left[\rho_m\left(T_\infty\right)\right]$ is the mass density of the bridge wire metal at ambient temperature T_∞, and T_{melt} is the melting temperature of the metal. Using these definitions, we deduce the following relationships:

$$\nabla^* = \left(\frac{\partial}{\partial x}\hat{i} + \frac{\partial}{\partial y}\hat{j} + \frac{\partial}{\partial z}\hat{k} \right) / \left[\frac{1}{a} \right] \tag{14}$$

$$\rho_m^* = \rho_m / \left\{ \frac{I_0^2 t_I^3}{\left[\sigma_e\left(T_\infty\right)\right] a^6} \right\} \tag{15}$$

$$k^* = k / \left\{ \frac{I_0^2}{\left[T_{\text{melt}} - T_\infty\right]\left[\sigma_e\left(T_\infty\right)\right] a^2} \right\} \tag{16}$$

$$c_v^* = c_{\text{v}} / \left\{ \frac{a^2}{t_I^2 \left[T_{\text{melt}} - T_\infty\right]} \right\} \tag{17}$$

$$\sigma_e^* = \sigma_e / \left[\sigma_e\left(T_\infty\right)\right] \tag{18}$$

$$E^* = E / \left\{ \frac{I_0^2 t_I^3}{\left[\sigma_e\left(T_\infty\right)\right] a^2} \right\} \tag{19}$$

$$V^* = V / \left\{ \frac{I_0^2 t_I^3}{\left[\sigma_e \left(T_\infty \right) \right] a} \right\} \tag{20}$$

$$I_0^* = \sin\left(2\pi t^* \right) \tag{21}$$

Substitution of equations 14 through 19 into equations 1 and 2 yields non-dimensional versions of the governing equations,

$$c_v^* \rho_m^* \frac{\partial T^*}{\partial t^*} = \sigma_e^* \left| E^* \right|^2 + \nabla^* \bullet (k^* \nabla^* T^*) \tag{22}$$

and

$$E^* \bullet \nabla^* \sigma_e^* + \sigma_e^* \nabla^* E^* = 0 . \tag{23}$$

2.2 Finite Element Implementation

Figure 1 shows the two-dimensional geometry implemented in ANSYS release 11 with a half bridge wire width of 0.5, and a length of 1. The width at the inlet and outlet regions of the "bow-tie" was 5, the angle of the inlet and outlet converging or diverging boundaries was 45°, and the fillet radius applied at the corners to the entrance of the bridge was 0.008. We modeled half the actual geometry to conserve computing resources, and applied the boundary conditions shown in figure 1.

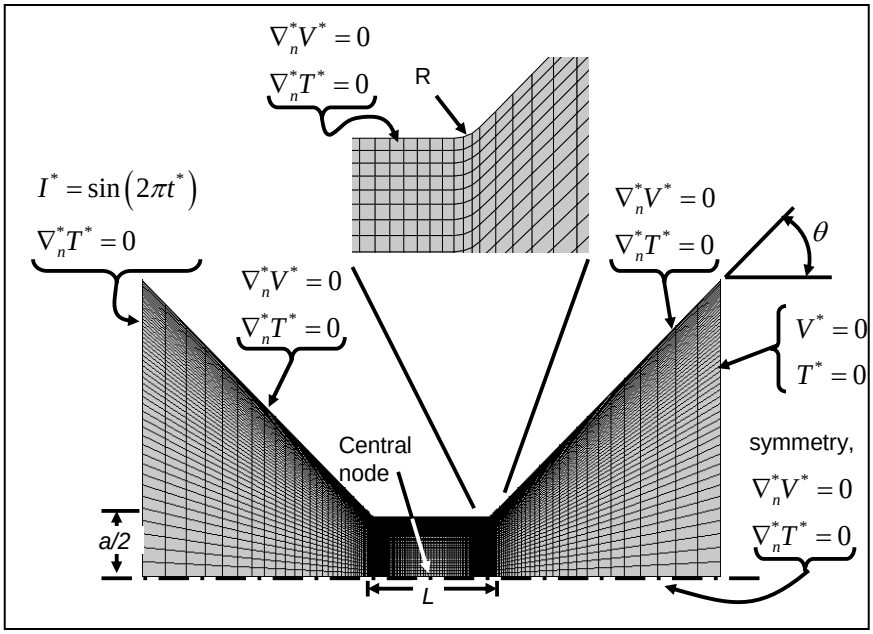

Figure 1. Finite element mesh, and boundary conditions of the fuze initiator geometry modeled. The symbol ∇_n^* refers to the gradient in the direction normal to the boundary.

We modeled three geometry and material combinations as shown in table 1. Cases 1 and 2 corresponded to those in (*5*, *6*), and case 3 corresponded to a single bridge foil of a multipoint wafer microfabricated at ARL. The current pulse amplitude for case 3 was 3800 A, which we assumed to be equally distributed among 15 bridge wires of the multi-point experiment shown in figure 2. Thus, the input current amplitude to a single wire was 253.3 A.

Table 1. Material and geometry combinations modeled.

Case	Material	Metal Thickness (μm)	Bridge Length (μm)	Input current pulse	
				Amplitude (A)	Period (ns)
1	Cu	1	1270	1200	588.2
2	Au	1	1270	1200	588.2
3	Cu	2.5	100	253.3	370

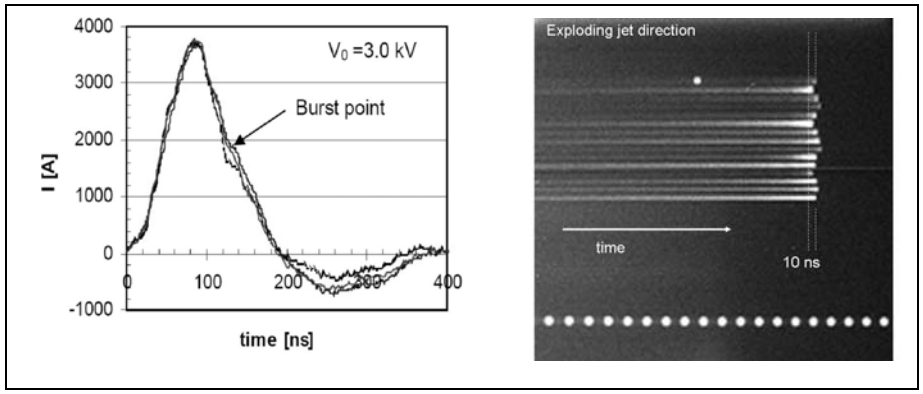

Figure 2. Experimental current pulse and streak photo from a multipoint initiation test performed at ARL.

We obtained thermal material properties for Cu and Au from (*8*). Figures 3 and 4 show the functional relationships for thermal conductivity k and specific heat c_v based on temperature. We obtained electrical conductivity in units of $1/\Omega m$ as a function of temperature T in units of Kelvin from (*3*), so that

$$\sigma_e\big|_{\mathrm{Cu}} = \left\{-4.12\times10^{-10} + 0.113\times10^{-5}\left(T/11604\right)^{1.145}\right\}^{-1} \tag{24}$$

for Cu, and

$$\sigma_e\big|_{\mathrm{Au}} = \left\{-4.95\times10^{-10} + 0.170\times10^{-5}\left(T/11604\right)^{1.178}\right\}^{-1} \tag{25}$$

for Au.

One important modification to the model inputs accounted for the fact that ANSYS assumes any 2-D thermal electrical elements to have a thickness d_1 of unity. The current density resulting from a current input I_0 to a line of 2-D nodes having a length a is I_0/ad_1. The actual 3-D case with current I_2 has finite depth d_2, so that the actual current density is I_2/ad_2. Equating current densities for the two cases yields $I_0 = I_2\left(d_1/a\right)\left(a/d_2\right)$. We readily recognize the quantity $\left(d_1/a\right)$ as the non-dimensionalized depth d_1^*, which is always unity in the ANSYS program. Thus, the current input I_0 to the ANSYS program for the real world, 3-D input I_2 must be scaled by the $\left(a/d_2\right)$ ratio:

$$I_0 = \frac{a}{d_2} I_2 . \tag{26}$$

These arguments are not necessary for a 3-D model, but are for a 2-D implementation as we have done for this report.

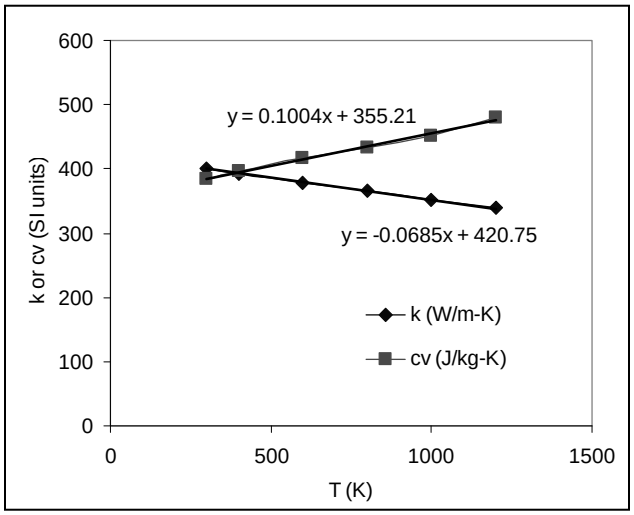

Figure 3. Thermal conductivity (k) and specific heat (cp) of Cu as a function of absolute temperature. Solid lines and equations in the form of $y = f(x)$ represent linear fits based on the least squares method.

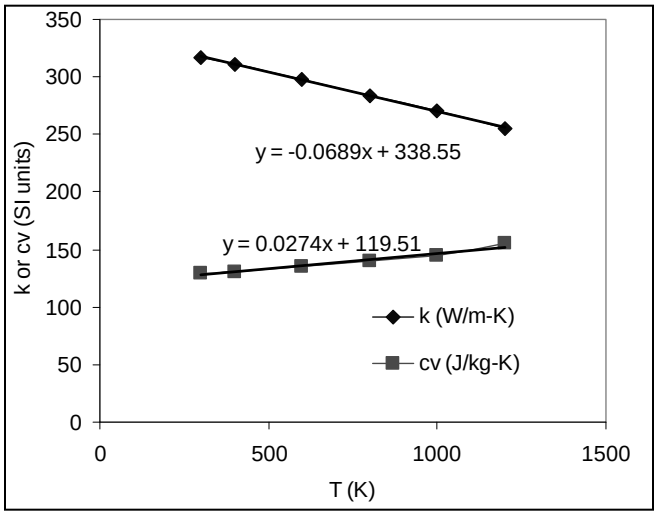

Figure 4. Thermal conductivity (k) and specific heat (cp) of Au as a function of absolute temperature. Solid lines and equations in the form of $y = f(x)$ represent linear fits based on the least squares method.

The transient solver of ANSYS attempted to automatically determine a time step size, but to control solution stability and to implement the current input waveform accurately we imposed a certain number of steps at which to force a solution (called "load steps" in the ANSYS program). First we estimated the time to melt by considering a lumped parameter approximation with constant material properties. With all spatial derivatives set equal to zero, equations 22 and 23 reduce to a single equation

$$c_v^* \rho_m^* \frac{\partial T^*}{\partial t^*} = \left| E^* \right|^2 . \tag{27}$$

Noting that $E^* = I_0^* / a^* d_1^* \sigma_e^*$, we set $E^* = I_0^*$ given our non-dimensional scheme. Thus, a quasi-static solution to equation 27 is

$$T^* = \frac{\left(I_0^* \right)^2}{c_v^* \rho_m^*} t^* \tag{28}$$

Equation 21 gives the relationship for I_0^*, and for small t^* we approximated equation 21 as

$$I_0^* \approx 2\pi t^* . \tag{29}$$

Substitution of equation 29 into 28 gives,

$$T^* \approx \frac{\left(2\pi t^* \right)^2}{c_v^* \rho_m^*} t^* . \tag{30}$$

Thus, the estimated time for T^* to reach the a melting temperature of 1 is

$$t_m^* \approx \left(\frac{c_v^* \rho_m^*}{4\pi^2} \right)^{1/3} . \tag{31}$$

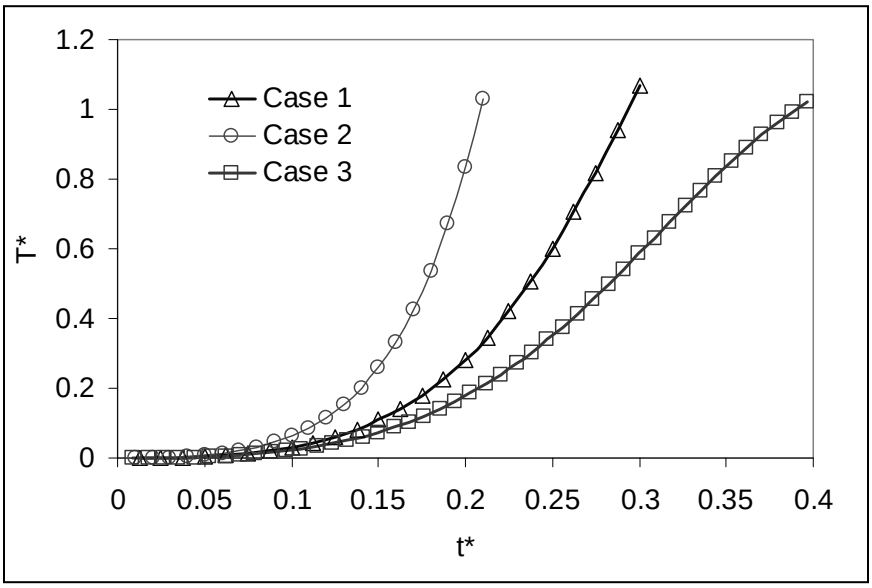

Figure 5. Non-dimensional temperature of the middle node versus non-dimensional time for the three cases in table 1. The melting temperature corresponds to $T^* = 1$, and time is scaled by the input current pulse period values in table 1.

We divided the quantity in equation 31 by 30 for the load step time in ANSYS, to insure approximately 30 load steps at which the program would calculate a solution leading up to the melting point of the center node of the bridge wire. Once a load step was reached where $T^* > 1$ for this node, we halted the solution and used a linear interpolation with the previous load step to approximate the exact time at which the temperature of this node exceeded the melting temperature.

3. Model Results

3.1 Transient Solutions

Figure 5 shows the temperature distribution versus time for the three cases in table 1. The shapes of the curves differ as melting time increased, with an increasing change in curvature near the end. A reason for this trend is the fact that, in the first quarter period of the input current pulse ($0 \le t^* \le 0.25$), the current and therefore rate of heating monotonically increased. During the second quarter period of the input sine wave ($0.25 \le t^* \le 0.5$), the current magnitude dropped, and the rate of heating logically followed the same trend.

Figure 6 shows the spatial temperature distribution at times that correspond approximately to case 3 central node temperatures of 0.3, 0.6, and 0.9. As in similar modeling studies, the current density increased greatly near the corners as a result of high electric fields, and therefore, the highest rate of heating occurred in the corners. The temperature then quickly spread throughout the rest of the bridge region.

The melting time of case 1 was within 1.5% of the predicted time in (*5*) for a similar set of geometry and material. This result increased our confidence that the model was implemented correctly, or at least as correctly as another previously published study. However, the melting time of case 2 was 39% longer than the time predicted in (*5*), and the melting time of case 3 was 22% longer than the experimentally-observed burst point. The actual melting time would be very difficult to determine experimentally for case 3 or any other cases due to the small sizes and short time scales involved.

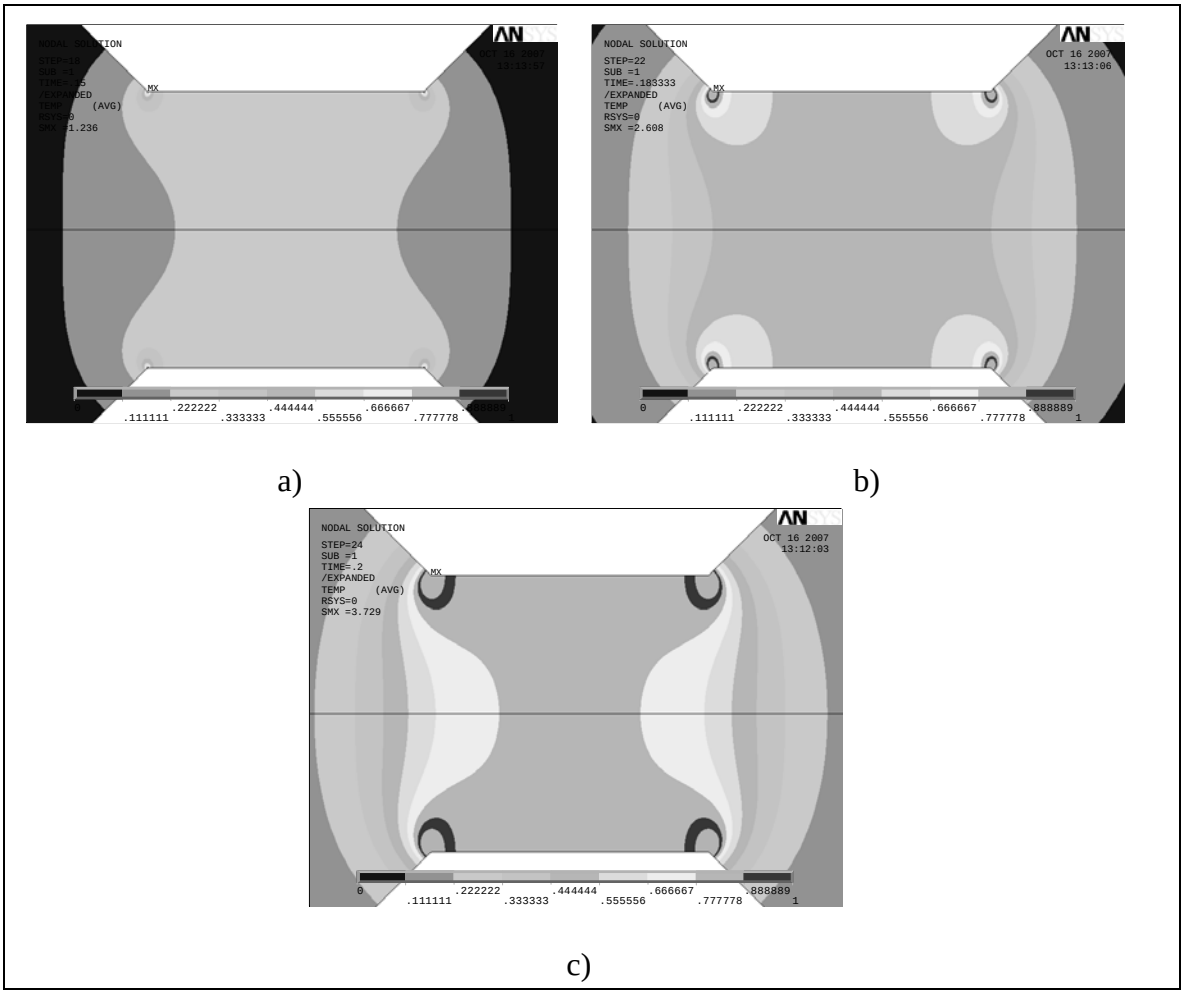

Figure 6. Temperature distribution of a Cu bridge foil for case 3 at a) t*=0.24, b) t*=0.31, and c) t*=0.36. The model results are reflected about the line of symmetry shown in figure 1.

To probe further into why the predicted value of Au differed so much from (*5*), figure 7 shows the current density near one of the corners. The vector pattern differed greatly from a plot at an equivalent time in (*5*), such that in figure 7 all vectors appear to have a negative or zero vertical component. In (*5*) some discussion is given about conductivity gradients near the corners giving rise to a constriction of the current stream right before melting, effectively increasing the corner radius of curvature. Current density vector plots show significant narrowing and then widening of the current stream, with significant positive current density vector components in the vertical direction. The effect is most pronounced for Au, but is present for all metals investigated in (*5*), including Cu.

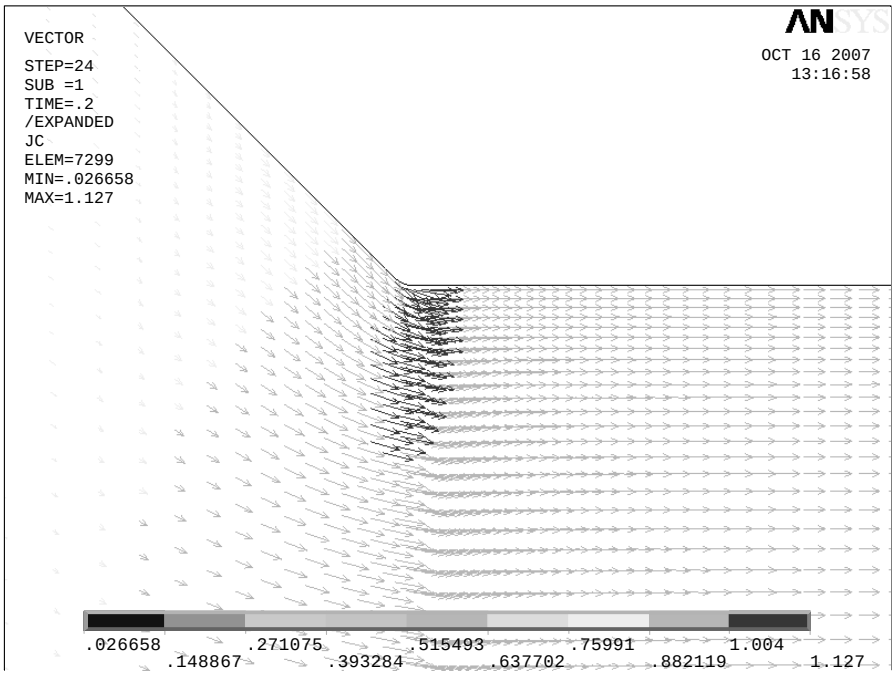

Figure 7. Current density at t*=0.20 for case 2, right before the center of sample reached the melting temperature.

These effects are not present in (*6*), and thus, although not explicitly stated in (*5*), the effects likely arise from a different electrical conduction model for temperatures above the melting point. A significant drop in conductivity beyond the melting temperature would produce large conductivity gradients and thus the vector plots shown in (*5*). In our model, we only extrapolate the conduction relationship given in equation 24 or 25, which when plotted is a nearly linear relationship changing by less than a factor of six over the temperature range $0 \le T^* \le 1$. Such gradual changes lead to relatively small conductivity gradients for the temperature distributions shown in figure 6, whereas gradients would be much larger with the empirically-observed order-of-magnitude changes in conductivity between solid and liquid phases.

3.2 Sensitivity Study

In order to investigate the effects of changing geometry and material parameters on the pre-melt behavior, we conducted a series of simulations for case 3 where we changed the bridge thickness d_2, bridge length L, corner radius R, taper angle θ, thermal conductivity k, mass density ρ_m, specific heat c_v, electrical conductivity σ_e, and melting temperature T_{melt} each by 5%. For those properties that varied with temperature, we applied the 5% change to the rate of change factor

(i.e., the linear slopes in figure 3 for c_v and k). We compared the time for the central node to reach the melting temperature to the original time to melt, and figure 8 shows the results. Interestingly, geometric factors such as taper angle and corner radius did not significantly affect the results, which we expected based on an early study of potential distributions (*9*). The thickness was expected to be a major factor because the thickness directly affects the applied current in equation 26. All material properties affected the time to melt except *k*, which was surprising until we considered the arguments below.

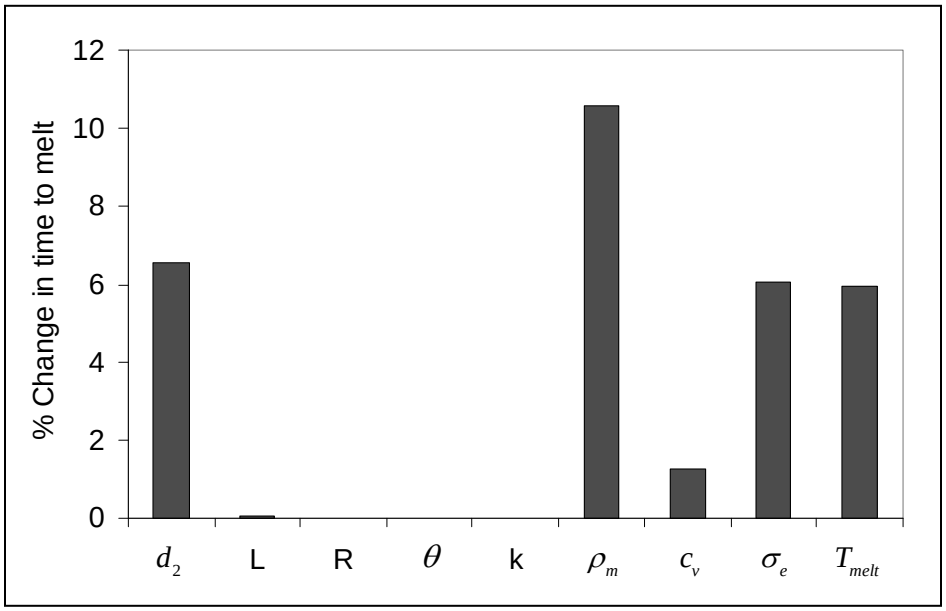

Figure 8. Percent change in time to melt resulting from 5% changes in individual geometric and material property variables.

The one-dimensional form of equation 22 with constant material properties is

$$\frac{c_v^* \rho_m^*}{k^*} \frac{\partial T^*}{\partial t^*} = \frac{I_0^{*2}}{k^*} + \frac{\partial^2 T^*}{\partial x^{*2}} . \tag{32}$$

A solution to the homogeneous solution (neglecting the forcing term I_0^{*2}) by separation of variables yields

$$T^*\left(x^*, t^*\right) = \exp\left(\frac{k^*}{c_v^* \rho_m^*} \frac{t^*}{\lambda^2}\right)\left[C_1 \cos\left(x^* / \lambda\right) + C_2 \sin\left(x^* / \lambda\right)\right] \tag{33}$$

where

$$\lambda^2 = 4 / n^2 \pi^2 \tag{34}$$

and *n* is any positive, non-zero integer. Neglecting spatial details, it is interesting to note the time constant τ of the exponential term,

$$\tau = \frac{4c_v^* \rho_m^*}{k^* \pi^2}. \tag{35}$$

Next we considered the steady state solution to equation 32 with boundary conditions of zero temperature flux at $x^* = 0$ and $T^* = 0$ at $x^* = 1$:

$$T^*\left(x^*, \infty\right) = \frac{I_0^{*2}}{2k^*}\left(1 - x^{*2}\right) \tag{36}$$

Equation 36 represents the final temperature if a current step input were applied, and equation 35 represents how quickly that temperature is attained. A hypothetical step response for $x^* = 0$ is

$$T^*\left(x^*, t^*\right) = \frac{I_0^{*2}}{2k^*}\left(1 - e^{-t^*/\tau}\right) \tag{37}$$

with an initial slope of

$$\frac{I_0^{*2}}{2k^*}\frac{k^* \pi^2}{4c_v^* \rho_m^*} = \frac{I_0^{*2} \pi^2}{8c_v^* \rho_m^*}. \tag{38}$$

For short times, an approximation of the solution is a linear line starting at $x^* = 0$ and extending upward with a slope given by equation 38. Thus, we expected the time to melt to be affected by changes in c_v, ρ_m but not k, and figure 8 demonstrates this expectation.

We note that the use of time for the central node to reach its melting temperature may not be the best parameter for a sensitivity study. Alternative figures of merit include the standard deviation of all nodes in the bridge region after a specified time, such as the time for the central node to reach the melting point or the time for the average of all bridge region nodes to reach the melting point. Such alternative figures of merit would indicate how changing input parameters might improve or impair temperature uniformity, which is expected to determine post melt behavior. Of course, the best figure of merit would be the time for the detachable flyer above the bridge wire to detach, or its final velocity after a certain distance, but such calculations are the subjects of future work.

4. Conclusions and Future Work

We have modeled the pre-melt behavior of an exploding foil initiator or slapper. The results in terms of time for the center of the exploding foil to reach the material melting temperature was within 2% of a similar, published modeling study, and approximately within 20% of the experimentally-observed time-to-burst for specific geometries fabricated at ARL. We performed a sensitivity study on several geometric and material properties, and found the melting time to be most sensitive to bridge wire thickness, and all material properties except thermal conductivity. We used simple, analytical arguments to explain these results.

Of course, the predicted melting time of one location in the bridge wire is not necessarily comparable to the experimental time to burst, and we anticipate two future technical reports detailing more complex models to treat post-melt behavior. We anticipate the next report to focus on the post-melt phase of the metal as it transitions from solid to liquid, with each finite element absorbing the latent heat of fusion and with material properties such as conductivity changing according to empirically-determined models. The liquid regions will then be free to expand and flow, requiring the coupling of a fluid mechanics code with the existing solid mechanics model. Portions of the model should quickly reach evaporation temperatures requiring another phase change into a gas. Finally, we anticipate the last technical report to cover the incorporation of a surrounding flyer material and substrate, which will allow accurately-modeled heat transfer and fluid-structure interaction as the bridge wire melts and expands. We plan to model the non-linear, plastic deformation of the flyer material either through an appropriate code allowing a fully-deformable mesh, or to investigate the possibility of modeling the problem with fluid mechanics using a hypothetical fluid with a large, non-Newtonian viscosity. It may also be possible to model the structure with a standard, linear stress-strain model, and to simply monitor when plastic deformation becomes too excessive to trust the results.

The path forward will result in a predictive model allowing any number of sensitivity studies. More importantly for model verification, model outputs will be available for direct comparison to experimental data such as time to burst and flyer velocity, and should greatly enhance our ability to design better bridge wire devices.

References

1. Zakar, E. *Fabrication technology for smart fuzes*; ARL-TR-3129; U.S. Army Research Laboratory: Adelphi, MD, Dec. 2003.

2. Zakar, E.; Mary, B.; Dubey, M.; Lee, U.; Mark, N.; Derenge, M. *Properties of Cr-Cu electrodes for advanced fuze development*; ARL-TR-4285; U.S. Army Research Laboratory: Adelphi, MD, Sept. 2007.

3. Burgess, T. J. "Electrical resistivity model of metals," Sandia National Laboratories, Supported under U. S. Dept. of Energy Contract No. DE-AC04-76DP00789.

4. Logan, J. D.; Lee, R. S.; Weingart, R. C.; Yee, K. S. Calculation of heating and burst phenomena in electrically exploded foils. *Journal of Applied Physic* **1977**, *48*, 621–628.

5. Baginski, M. E.; Shaffer, E. C.; Thomas, K. A.; McGuirk, J. S. A comparison of the electrodynamics of metal under the action of large electric currents. *Inter. J. Applied Electromagnetics and Mechanics* **2000**, *11*, 79–93.

6. Baginski, M. E.; Baginski, T. A.; Thomas, K.; Shaffer, E. C. A comparison of the electrodynamics of metal under the action of large electric currents. *Inter. J. Applied Electromagnetics and Mechanics* **1996**, *7*, 193–202.

7. Richardson, D. D. *The uniformity of heating of foil bridges in multiple configurations*; AFATL-TR-85-27; Air Force Armament Laboratory: Eglin AFB, FL, May 1985.

8. Incropera, F. P.; Dewitt, D. P. *Introduction to heat transfer*, 3rd ed.: John Wiley & Sons, 1996.

9. Richardson, D. D. Calculations of electrical properties of thin metal bridge foils using the boundary element method. *Engineering Analysis* **1985**, *1*, 195–199.

Appendix. ANSYS Input File Listing

```
/CWD,'C:\Documents and Settings\christopher.morris17\My Documents\projects\fuzing\ansys'
!/CWD,'C:\Documents and Settings\christopher.morris17\My Documents\Runspace'
/FILNAME,fuze_2d_45tap_0p08fillet_Cu,1

!The problem is as follows:
  thk = 2.5e-6 !m
  a = .1e-3 !m
  I0 = 3800*(a/thk)/15 !Amps
  t_I = 370e-9 !s
  T_inf = 300 !K
  eV_to_K = 11604 !K/eV

! Non-dimensional temperatures at which to evaluate properties
  T1=0
  T2=0.05
  T3=0.1
  T4=0.5
  T5=1
  T6=5

! Thus, the non-dimensional values become:
a_star=1
I0_star=1   !Current input amplitude


br_len = a_star
br_wid = a_star
in_wid = 5*a_star
out_wid = in_wid
taper = 45  ! degrees
fillet = 0.08*a_star

br_mat = 1  !1=Cu, 2=Au

e_size = a_star/30
ndivb = 100 ! number of horizontal element divisions in the bridge
```

```
! ------------------------------------------------------------------
! ---------- BUILDING MODEL ----------------------------------------
! ------------------------------------------------------------------

/PREP7          !Enter the preprocessor

! First, delete all previous geometry, if it's there...
ALLSEL
ACLEAR,ALL
ADELE,ALL,,,1
ldele,all,,,1
kdele,all,,,1
!/NERR,0,10000                          !Supress warning messages
/triad,off
/PNUM,KP,0
/PNUM,LINE,1
/PNUM,AREA,0
/PNUM,VOLU,0
/PNUM,NODE,0
/PNUM,SVAL,0
/PNUM,ELEM,0
/NUM,0

!---------------------------------------
!** MATERIAL PROPERTIES **
!---------------------------------------
TOFFST,0  ! Temperature offset from absolute zero (don't let ANSYS apply any other offsets)
EMUNIT,EPZRO,1   ! I don't think permittivity is used in these calculations, but I'll set
                 !it to a non-dimensional value of 1 anyway
                 !(like I would for electrostatic analyses).
!Material 1: Copper

T_melt = 1358 !K
rho_m = 8920 !kg/m^3
!--Coeff.'s from Burgess resistivity model
C1 = -4.12e-5
C2 = 0.113
C3 = 1.145
! Coef's on fits for Cv(T), k(T)
cv3 = 0
cv2 = 0
cv1 = 0.1004
cv0 = 355.21
```

```
k1 = -0.0685
k0 = 420.75

sigma_0=100000/(C1+C2*((T_inf/eV_to_K)**C3))
UIMP,1,DENS,,,rho_m/( ((I0**2)*(t_I**3)) / (sigma_0*(a**6)) )
Tdim1=T1*(T_melt-T_inf)+T_inf
Tdim2=T2*(T_melt-T_inf)+T_inf
Tdim3=T3*(T_melt-T_inf)+T_inf
Tdim4=T4*(T_melt-T_inf)+T_inf
Tdim5=T5*(T_melt-T_inf)+T_inf
Tdim6=T6*(T_melt-T_inf)+T_inf

! Specific heat
MPTEMP,,,,,,,,
MPTEMP,1,T1
MPTEMP,2,T2
MPTEMP,3,T3
MPTEMP,4,T4
MPTEMP,5,T5
MPTEMP,6,T6
MPDELE,C,1
MPDATA,C,1,,(cv3*Tdim1**3 + cv2*Tdim1**2 + cv1*Tdim1 + cv0)
/((a**2)/(t_I**2*(T_melt-T_inf)))
MPDATA,C,1,,(cv3*Tdim2**3 + cv2*Tdim2**2 + cv1*Tdim2 + cv0)
/((a**2)/(t_I**2*(T_melt-T_inf)))
MPDATA,C,1,,(cv3*Tdim3**3 + cv2*Tdim3**2 + cv1*Tdim3 + cv0)
/((a**2)/(t_I**2*(T_melt-T_inf)))
MPDATA,C,1,,(cv3*Tdim4**3 + cv2*Tdim4**2 + cv1*Tdim4 + cv0)
/((a**2)/(t_I**2*(T_melt-T_inf)))
MPDATA,C,1,,(cv3*Tdim5**3 + cv2*Tdim5**2 + cv1*Tdim5 + cv0)
/((a**2)/(t_I**2*(T_melt-T_inf)))
MPDATA,C,1,,(cv3*Tdim6**3 + cv2*Tdim6**2 + cv1*Tdim6 + cv0)
/((a**2)/(t_I**2*(T_melt-T_inf)))
! Thermal conductivity
MPTEMP,,,,,,,,
MPTEMP,1,T1
MPTEMP,2,T2
MPTEMP,3,T3
MPTEMP,4,T4
MPTEMP,5,T5
MPTEMP,6,T6
MPDELE,KXX,1
MPDELE,KYY,1
MPDATA,KXX,1,,(k1*(T1*(T_melt-T_inf)+T_inf)+k0)/((I0**2)/((T_melt-
```

```
T_inf)*sigma_0*a**2))
MPDATA,KXX,1,,(k1*(T2*(T_melt-T_inf)+T_inf)+k0)/((I0**2)/((T_melt-
T_inf)*sigma_0*a**2))
MPDATA,KXX,1,,(k1*(T3*(T_melt-T_inf)+T_inf)+k0)/((I0**2)/((T_melt-
T_inf)*sigma_0*a**2))
MPDATA,KXX,1,,(k1*(T4*(T_melt-T_inf)+T_inf)+k0)/((I0**2)/((T_melt-
T_inf)*sigma_0*a**2))
MPDATA,KXX,1,,(k1*(T5*(T_melt-T_inf)+T_inf)+k0)/((I0**2)/((T_melt-
T_inf)*sigma_0*a**2))
MPDATA,KXX,1,,(k1*(T6*(T_melt-T_inf)+T_inf)+k0)/((I0**2)/((T_melt-
T_inf)*sigma_0*a**2))
! Resistivity
MPTEMP,,,,,,,,
MPTEMP,1,T1
MPTEMP,2,T2
MPTEMP,3,T3
MPTEMP,4,T4
MPTEMP,5,T5
MPTEMP,6,T6
MPDELE,RSVX,1
MPDELE,RSVY,1
MPDATA,RSVX,1,,1/(100000/(C1+C2*( ((T1*(T_melt-T_inf)+T_inf) / eV_to_K)**C3)
)/sigma_0)
MPDATA,RSVX,1,,1/(100000/(C1+C2*( ((T2*(T_melt-T_inf)+T_inf) / eV_to_K)**C3)
)/sigma_0)
MPDATA,RSVX,1,,1/(100000/(C1+C2*( ((T3*(T_melt-T_inf)+T_inf) / eV_to_K)**C3)
)/sigma_0)
MPDATA,RSVX,1,,1/(100000/(C1+C2*( ((T4*(T_melt-T_inf)+T_inf) / eV_to_K)**C3)
)/sigma_0)
MPDATA,RSVX,1,,1/(100000/(C1+C2*( ((T5*(T_melt-T_inf)+T_inf) / eV_to_K)**C3)
)/sigma_0)
MPDATA,RSVX,1,,1/(100000/(C1+C2*( ((T6*(T_melt-T_inf)+T_inf) / eV_to_K)**C3)
)/sigma_0)


!-----------------------------------------------
!-------------End of Material props
!-----------------------------------------------
*AFUN,deg

        K,1,-br_len/2 -(out_wid/2-br_wid/2)/tan(taper), +out_wid/2
        K,2,-br_len/2,br_wid/2
        K,3,br_len/2,br_wid/2
        K,4,br_len/2 + (out_wid/2 - br_wid/2)/tan(taper), +out_wid/2
```

```
L,1,2
L,2,3
L,3,4
LFILLT,1,2,fillet
LFILLT,2,3,fillet

k,2,-br_len/2 -(out_wid/2-br_wid/2)/tan(taper),0   !KP #2 got replaced by 5,6

*get,xcoord,kp,5,loc,x
K,9,xcoord,0
*get,xcoord,kp,6,loc,x
K,10,xcoord,0
*get,xcoord,kp,7,loc,x
K,11,xcoord,0
*get,xcoord,kp,8,loc,x
K,12,xcoord,0

K,3,br_len/2 + (out_wid/2 - br_wid/2)/tan(taper),0 !KP #3 got replaced by 5,6


L,1,2
L,2,9
L,9,10
L,10,11
L,11,12
L,12,3
L,4,3

L,5,9
L,6,10
L,7,11
L,8,12

!Create Areas
AL,1,6,7,13          !1
AL,8,14,4,13         !2
AL,9,15,2,14         !3
AL,10,16,5,15        !4
AL,11,12,3,16        !5


lsel,s,line,,12,16
lsel,a,line,,6
```

```
        lesize,all,,,ndivb/2,10          !vertical lines
        lsel,s,line,,4,8,4
        lsel,a,line,,5,10,5
        *if,nint(fillet*ndivb),eq,0,then
                lesize,all,,,3                          !fillet lines
        *else
                lesize,all,,,3*NINT(fillet*ndivb)               !fillet lines
        *endif
        lsel,s,line,,2,9,7
        lesize,all,,,ndivb,-10   !horizontal lines in bridge
        lsel,s,line,,1,7,6
        lesize,all,,,40,1/60     !horizontal lines leading into bridge
        lsel,s,line,,3,11,8
        lesize,all,,,40,60       !horizontal lines leading into bridge

        allsel

!-----------------
!Select areas and assign attributes
!-----------------

        !Set element types
        ET,1,PLANE223,110

        !-select membrane areas
        ASEL,S,AREA,,1,5
        AATT,br_mat,1,1,0

        ! ** Mesh **
        ESHAPE,2     !Use mapped mesh

        ESIZE,e_size
        ASEL,S,area,,1,5
        AMESH,ALL

allsel

! ------------------------------------------------------------------------
! ----------- END OF BUILDING MODEL ----------------------------------
! ------------------------------------------------------------------------


!----------------------------------
!-- SOLUTION
```

```
!-----------------------------------
/solu
ANTYPE,TRANS,NEW
! Apply initial conditions to all nodes:
IC,all,TEMP,0
IC,all,volt,0
KBC,0   ! ramped boundary conditions
OUTRES,ERASE

*afun,rad
PI=ACOS(-1)
tstep= (1+T_inf/(T_melt-T_inf))
tstep=tstep*(cv1*Tdim1+cv0)*(t_I**2)*(T_melt-T_inf)/(a**2)
tstep=tstep*rho_m*sigma_0*(a**6)/(I0**2)/(t_I**3)
tstep=tstep/4/(PI**2)
tstep=tstep**(1/3)
tstep=tstep/30
t_total = .5

!-----------------------------
*do,ls,tstep,t_total,tstep

time,ls

/com,
/com,
/com,
/com,
/com, incrementing ls
/com,
/com,
/com,
/com,
!-----------------
!Apply BCs
!-----------------
lsel,s,line,,1,5
nsll,s,1
f,all,amps,0
f,all,heat,0
lsel,all

nsel,s,loc,y,0,0
f,all,amps,0
```

```
f,all,heat,0       !symmetry BC
*afun,deg
nsel,s,loc,x,br_len/2 + (out_wid/2 - br_wid/2)/tan(taper)
d,all,volt,0
d,all,temp,0

nsel,s,loc,x,-br_len/2 -(out_wid/2-br_wid/2)/tan(taper),-br_len/2 -(out_wid/2-
br_wid/2)/tan(taper)
nsel,u,loc,y,out_wid/2,out_wid/2
*get,my_b,node,,mxloc,y
*GET,nodes,NODE,0,count
*afun,rad
PI=ACOS(-1)
Iin=I0_star*sin(2*PI*ls)
f,all,amps,0.5*Iin/nodes/(1-((out_wid/2 - my_b)/(out_wid/2)))  ! Current is applied so
                                                    ! the total current into the bridge is Iin.  The
                                                    ! factor of 0.5 accounts for symmetry.  The other
                                                    ! factors account for not applying current to
                                                    ! "walls"
f,all,heat,0


allsel

TRNOPT,FULL
LUMPM,0
!*
!OUTRES,ALL,1
!OUTRES,nsol,last

solve

/post1
!SET,LAST  !read last set
nsel,s,loc,x,0,0
nsel,r,loc,y,0,0
*get,nodenum,node,,num,max
*get,myTemp,node,nodenum,temp
*if,myTemp,gt,1,exit      ! Stop after the melting temperature is reached
allsel
/solu
antype,,rest  ! restart the analysis

*enddo
```

```
!------------------------------

!-----------------------------------
!-- END OF SOLUTION
!-----------------------------------

/post1

! interpolate time to melt:
SET, NEAR,,,,LS-tstep
*get,T_last,node,nodenum,temp
tm_star = (1-T_last)*(tstep/(myTemp-T_last)) + (LS-tstep)
set,last

/EXPAND,2,RECT,HALF,,0.00001
PLNSOL, temp,, 0
/AUTO,1
/ZOOM,1,SCRN,0.340024,0.006081,0.596081,-0.210017

*if,1,eq,0,then
PLNS,TEMP,
ANTIME,50,0.2, ,1,2,0,0.5
*endif

/POST26
!FILE,'fuze_2d','rst','.'
/UI,COLL,1
NUMVAR,200
SOLU,191,NCMIT
STORE,MERGE
FILLDATA,191,,,,1,1
REALVAR,191,191
!*
nsel,s,loc,x,0,0
nsel,r,loc,y,0,0
*get,nodenum,node,,num,max
NSOL,2,nodenum,TEMP,, TEMP_2
STORE,MERGE
XVAR,1
PLVAR,2,
allsel
FINISH
```

INTENTIONALLY LEFT BLANK

Distribution List

NO. COPIES	ORGANIZATION
1 (ELECTRONIC COPY)	ADMNSTR DEFNS TECHL INFO CTR ATTN DTIC-OCP 8725 JOHN J KINGMAN RD STE 0944 FT BELVOIR VA 22060-6218
1	DARPA ATTN IXO S WELBY 3701 N FAIRFAX DR ARLINGTON VA 22203-1714
1	OFC OF THE SECY OF DEFNS ATTN ODDRE (R&AT) THE PENTAGON WASHINGTON DC 20301-3080
1	US ARMY RSRCH DEV AND ENGRG CMND ARMAMENT RSRCH DEV AND ENGRG CTR ARMAMENT ENGRG AND TECHNLGY CTR ATTN AMSRD-AAR-AEF-T J MATTS BLDG 305 ABERDEEN PROVING GROUND MD 21005-5001
1	US ARMY TRADOC BATTLE LAB INTEGRATION & TECHL DIRCTRT ATTN ATCD-B 10 WHISTLER LANE FT MONROE VA 23651-5850
1	SMC/GPA 2420 VELA WAY STE 1866 EL SEGUNDO CA 90245-4659
1	US ARMY INFO SYS ENGRG CMND ATTN AMSEL-IE-TD F JENIA FT HUACHUCA AZ 85613-5300
1	COMMANDER US ARMY RDECOM ATTN AMSRD-AMR W C MCCORKLE 5400 FOWLER RD REDSTONE ARSENAL AL 35898-5000
1	US ARMY RSRCH LAB ATTN AMSRD-ARL-CI-OK-TP TECHL LIB T LANDFRIED BLDG 4600 ABERDEEN PROVING GROUND MD 21005-5066
5	US ARMY TACOM-ARDEC ATTN AMSRD-AAR-AE R FONG ATTN AMSRD-AAR-AEE-W B NG ATTN AMSRD-AAR-AEE-W J OROSZ ATTN AMSRD-AAR-AEE-W S TANG ATTN AMSRD-AAR-AEE-W V GOLD BLDG 3022 PICATINNY ARSENAL NJ 07806
1	US ARMY TACOM-ARDEC ATTN AMSRD-AAR-AEP-F B HUBAL BLDG 6 PICATINNY ARSENAL NJ 07806
1	US ARMY TACOM-ARDEC ATTN AMSRD-AAR-AEE-W E BAKER BLDG 3022 PICATINNY ARSENAL NJ 07806-5000

NO. COPIES	ORGANIZATION
1	US ARMY TACOM-ARDEC ATTN AMSRD-AAR-AEP-F P GORMAN BLDG 6 PICATINNY ARSENAL NJ 07806-5000
1	NAVAL AIR WARFARE CENTER ATTN CODE 478C00D G HENNINGS CHINA LAKE CA 93555-5000
1	NAVAL SURFACE WARFARE CENTER DAHLGREN DIVISION ATTN CODE G22 B HANNA 17320 DAHLGREN RD DAHLGREN VA 22448-5100
2	AFRL/MNMF ATTN D MABRY ATTN E WILD 306 W EGLIN BLVD BLDG 432 EGLIN AFB FL 32542-5430
1	LOS ALAMOS NATL LAB ATTN K THOMAS PO BOX 1663 LOS ALAMOS NM 87545
1	SANDIA NATL LAB ATTN S HARRIS PO BOX 5800 ALBUQUERQUE NM 87185-1452
1	US GOVERNMENT PRINT OFF DEPOSITORY RECEIVING SECTION ATTN MAIL STOP IDAD J TATE 732 NORTH CAPITOL ST., NW WASHINGTON DC 20402

NO. COPIES	ORGANIZATION
1	DIRECTOR US ARMY RSRCH LAB ATTN AMSRD-ARL-RO-EV W D BACH PO BOX 12211 RESEARCH TRIANGLE PARK NC 27709
15	US ARMY RSRCH LAB ATTN AMSRD-ARL-CI-OK-T TECHL PUB (2 COPIES) ATTN AMSRD-ARL-CI-OK-TL TECHL LIB ATTN AMSRD-ARL-D J M MILLER ATTN AMSRD-ARL-SE RL C MORRIS (3 COPIES) ATTN AMSRD-ARL-SE-D E SHAFFER ATTN AMSRD-ARL-SE-R P AMIRTHARAJ ATTN AMSRD-ARL-SE-RL E ZAKAR ATTN AMSRD-ARL-SE-RL M DUBEY ATTN IMNE-ALC-IMS MAIL & RECORDS MGMT ATTN AMSRD-AAR-AEP-F(A) B MARY ATTN AMSRD-AAR-AEP-F (A) D ERRERA ATTN AMSRD-AAR-AEP-F (A) W KONICK ADELPHI MD 20783-1197